Tutor/s

Dr. Jordi Cirera Fernández

Departament de Química Inorgànica i Orgànica

Secció de Química Inorgànica

Grau de Química

Treball Final de Grau

Development of a first principles force field for metal-organic [Fe_4] cages.

Desenvolupament d'un camp de forces per primers principis per gàbies metal·lo-orgàniques de [Fe_4].

Laia Navarro Maestro

June 2019

Universitat de Barcelona

B:KC Barcelona Knowledge Campus
Campus d'Excel·lència Internacional

Nothing in life is to be feared, it is only to be understood. Now is the time to understand more, so that we may fear less.

Marie Curie

Acknowledgements:

To Dr. Cirera for guiding and supporting me over this final degree project, and for providing me criterion, knowledge and having increased my critical spirit. I'm very grateful that you have introduced me to the world of computational chemistry; it has been a pleasure.

To Dr. Jover for his help, advice and kind welcome.

To my family and friends for the support and constant encouragement they have given me over the years.

REPORT

CONTENTS

1. SUMMARY

Metal-organic cages (MOCs) containing four Fe(II) metal centres ([Fe_4]) represent a novel class of molecules that have attracted a lot of interest due to, among others, its efficiency in encapsulating greenhouse gases such as SF_6. On the top of that, the [Fe_4] molecules exhibit spin-crossover (SCO) behaviour, which can be tuned as a function of the guest molecule encapsulated in the system. Due to their size, conventional electronic structure calculations are not suited to study the origin of such interaction and its effect on the SCO behaviour and different computational methodologies need to be developed in order to study the nature of the host-guest interaction.

First, by performing DFT calculations, the Fe-N bond will be modelled using a Morse potential. This data will be adjusted simultaneously against an energy scan along the totally symmetric normal mode in order to generate an *ab initio* force field for the molecule. Also, a series of electronic structure calculations will be carried out at CASSCF/NEVPT2 level to extract the relevant Angular Overlap Model parameters for a very simple molecule, $[Fe(NH_3)_6]^{2+}$, representative of the Fe(II) environment in [Fe_4] MOCs; necessary to construct the force field.

In order to see if the results of $[Fe(NH_3)_6]^{2+}$ can be extrapolated to more complex systems like the [Fe_4] cages, the ammonia results will be compared with systems of increasing complexity yet closely related to the actual Fe environment in the [Fe_4] system: $[Fe(py)_6]^{2+}$ and $[Fe(C_6H_6N_2)_3]^{2+}$. Once validated, then the complete force field for the [Fe_4] system will be assembled and tested.

Finally, LFMM simulations will be run in the NVE, NVT or NPT/NσT ensemble to study the interaction between the [Fe_4] system and the SF_6 molecule in a large enough system so the crystal packing effects can be properly modelled.

Keywords: force field, electronic structure, transition metals, molecular mechanics, Ligand-Field Molecular Mechanics, ab initio ligand field theory, angular overlap model, density functional theory, LFMM, AILFT, AOM, DFT

2. RESUM

Les gàbies metal·lo-orgàniques (MOCs) que contenen quatre centres de Fe(II) ([Fe_4]) representen una nova classe de molècules d'interès a causa, entre altres, de la seva eficàcia en l'encapsulament de gasos d'efecte hivernacle com el SF_6. A més, mostren un comportament de transició de spin (SCO) el qual pot ser ajustat en funció de la molècula hoste encapsulada en el sistema. Amb motiu de la seva mida, els càlculs d'estructura electrònica convencionals no són adequats per estudiar l'origen d'aquesta interacció i el seu efecte en el comportament de SCO, i cal desenvolupar diferents metodologies computacionals per estudiar la naturalesa de la interacció host-guest.

Realitzant càlculs DFT es modelitzarà l'enllaç Fe-N utilitzant un potencial de Morse. Aquestes dades s'ajustaran simultàniament enfront un escanejat d'energia al llarg del mode normal totalment simètric, amb l'objectiu de generar un camp de forces *ab initio* per a la molècula. També es duran a terme una sèrie de càlculs d'estructura electrònica a nivell de CASSCF/NEVPT2 per extreure els paràmetres rellevants de l'AOM per a una molècula molt simple, $[Fe(NH_3)_6]^{2+}$, representativa de l'ambient del Fe(II) en les MOCs de [Fe_4]; necessaris per construir el camp de forces.

Per veure si els resultats del $[Fe(NH_3)_6]^{2+}$ es poden extrapolar a les gàbies de [Fe_4], aquests es compararan amb sistemes de complexitat creixent estretament relacionats amb l'entorn real del Fe en el sistema de [Fe_4]: $[Fe(py)_6]^{2+}$ i $[Fe(C_6H_6N_2)_3]^{2+}$. Llavors, el camp de forces complet pel sistema de [Fe_4] serà muntat i testejat: s'executaran simulacions de LFMM en el conjunt NVE, NVT o NPT/NσT per estudiar la interacció entre les gàbies de [Fe_4] i el SF_6 en un sistema prou gran com per poder modelitzar adequadament els efectes de l'empaquetament del cristall.

Paraules clau: camp de forces, estructura electrònica, metalls de transició, mecànica molecular, Ligand-Field Molecular Mechanics, ab initio ligand field theory, model de solapament angular, teoria del funcional de la densitat, LFMM, AILFT, AOM, DFT

3. INTRODUCTION

Biological processes present host-guest chemistry, involving molecular recognition through non-covalent interactions (as for example when substrates bind to enzymes).[1] Considerable attention has been paid to the construction of container molecules such as self-assembled coordination cages in recent years for their wide-ranging applications in separation, molecular recognition, catalysis, gas storage, stabilization of reactive species, modulation of encapsulated guest reactivity and other applications. Metal-organic cages (MOCs) with porous surfaces and abundant recognition sites in their central cavities can typically bind guest molecules through specific host-guest interactions and molecular recognition.

3.1. [Fe_4] SYSTEMS AND APPLICATIONS, SF_6 CAPTURE AND SPIN-CROSSOVER

MOCs containing four iron metal centres ([Fe_4]) represent a novel class of molecules that have interest due to its efficiency in encapsulating greenhouse gases such as SF_6.[2] A greenhouse gas is a gas that has strong absorption bands in the infrared region interacting strongly with the thermal radiation emitted from the Earth's surface and cause the greenhouse effect which is a process that warms the Earth's surface.[3]

These [Fe_4] molecules exhibit spin-crossover (SCO) behaviour, which can be tuned as a function of the guest molecule encapsulated in the system. Spin crossover (SCO) within Fe(II) complexes is a phenomenon of interest. Due to its applications in molecular switching, memory and display devices, SCO in supramolecular structures has been explored in molecular frameworks, polymeric materials, and discrete multinuclear complexes.[4][5][6]

In this study, a first principle force field (FF), based on the Ligand-Field Molecular Mechanics (LFMM) approach will be developed for a particular [Fe_4] system, in order to study its interaction with the SF_6 molecule.

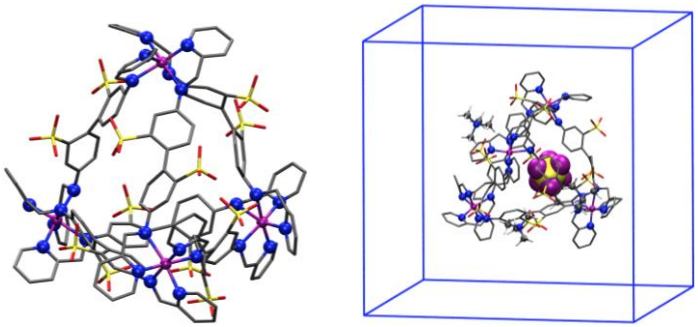

Figure 1.Global [Fe_4] system of study. Left: [Fe_4] empty cage without counter ions; Right: [Fe_4] cage with the guest molecule (SF_6) and the counter ions ($[N(CH_3)_4]^+$).

3.2. LIMITATIONS OF ELECTRONIC STRUCTURE METHODS TO STUDY [Fe_4]

Inherently, studying a system with open shells using electronic structure methods is difficult, and it is also difficult to describe coordination metal systems due to their variety of oxidation states, spin states and coordination numbers. Moreover, the classical study of electronic structure of this type of compounds is not useful because the system of study is very large. Classical studies using electronic structure methods are not powerful enough to study systems beyond 200 atoms.[7][8] Being so large the options that we would have at the level of electronic structure would be very expensive. Although we could perform a Density Functional Theory (DFT) calculation at a specific level, which would take a very long computational time, the results would not help much because the interest of this project is in the study of the molecular dynamics and the temporal evolution of the system. A static photography of the system is not of interest.

It is possible to solve this limitation by using a force field (FF) method approach. A FF constructs a parameterized potential energy surface from experimental or calculated data. After this point, we are able to study how the system evolves as a function of time. In our case, we construct a FF based on the Generalized Amber Force Field (GAFF)[9], but since these parameters do not exist to describe the Fe-N bond, we must build the corresponding force field to this interaction by first principles (Fe-N interactions are not in Generalized Amber Force Field (GAFF), Chemistry at Harvard Macromolecular Mechanics (CHARMM), or any commercial force field).

Hence, the parameters for Fe(II) must be built from first principles. How is it done?

We need to calculate the parameters of the Angular Overlap Model, AOM.[10] To calculate these parameters we need the *Ab Initio Ligand Field Theory* (AILFT) calculations. Complete Active Space Self-Consistent Field/second-order N-Electron Valence Perturbation Theory (CASSCF/NEVPT2) calculations are performed.[7][8][11] Then, these results are translated with AILFT, which is what gives us the splitting of the d orbitals. It is necessary to perform an energy scan and fit a Morse potential to describe the bond within AOM. If the Morse potential is not added and we only have the AOM parameters, which leads to an attractive potential, the molecule collapses. Morse potential adds this repulsive part necessary to have a stable system in its equilibrium geometry so that the system oscillates around the equilibrium position.

In order to carry out the AILFT calculations, an optimization calculation at a DFT level is needed, obtaining the optimized geometry, the charges and the frequencies.

4. OBJECTIVES

The main objective of this final degree project is to study the dynamic processes that take place once the [Fe_4] cage system encapsulates the guest SF_6 molecule as a function of time and at different temperatures. To achieve this, it is necessary to carry out several procedures:

1. Develop a force field by first principles that describes the Fe-N bond.
2. Build a force field for the empty [Fe_4] cage system.
3. Prepare and balance the global [Fe_4] cage system with the host molecule and the counter ions.
4. Analyse different trajectories at different temperatures to see how the SF_6 molecule behaves within the [Fe_4] system.

5. METHODOLOGY

To achieve the objectives mentioned above, it is necessary to perform a series of calculations at different levels of complexity using different tools from theoretical chemistry. These tools will be explained hereunder.

DFT methods do not reproduce well enough the exchange and correlation interactions. To solve this problem, we can use multireference methods such as CASSCF and NEVPT2.[11]

The methods used in this study provide electron correlation, which is usually divided into dynamic and static correlation. The dynamic correlation has to do with the movement of the electrons; it is the interaction between one electron and the electrostatic potential generated by the other electrons. The static correlation is important for molecules in which the ground state cannot be described by a single determinant, and appears due to the multiconfigurational character of the system and depends on its nature.[7][8][11]

5.1. DENSITY FUNCTIONAL THEORY (DFT)

DFT is a computational quantum mechanical modelling method used to investigate the electronic structure, principally the ground state, of many-body systems.[7][8][12][13] Applied to electronic systems, is a variational procedure alternative to the solution of the Schrödinger equation, alternative to traditional *ab initio* methods based on the wave function, where the functional of electronic energy is minimized with respect to electronic density.

Using this theory, the properties of a many-electron system can be determined by using functionals. A functional is a function whose variable is another function.

Computational costs are relatively low when compared to traditional methods. The main advantage of the DFT methods is that they are much simpler from the computational point of view because the electronic density, ρ, is a function of 3 variables: depends only on the x, y, z coordinates of the individual electron. It also allows to introduce the electronic correlation using exchange-correlation functionals.

These methods use the Hohenberg-Kohn theorem, which shows the existence of a functional that determines the energy of the ground state and the electronic density exactly. However, the theorem does not provide the form of the functional. Thus, the main problem is to find the correct form of the functional to use. Some approximate functionals are known that give quite good results in a range of chemical problems.

It is one of the most used methods in the quantum calculations of electronic structures.

5.2. MULTIREFERENCE METHODS (CASSCF/NEVPT2)

Multi-Configurational Self-Consistent Field (MCSCF) is a method in quantum chemistry used to generate correct reference states of molecules in cases where Hartree-Fock (HF) and DFT are not adequate.[7][8][11] It uses a linear combination of configuration state functions (CSFs), or configuration determinants, to approximate the exact electronic wavefunction of an atom or molecule. The set of coefficients of both the CSFs or determinants and the basis functions in the molecular orbitals, are varied to obtain the total electronic wavefunction with the lowest possible energy. This method is a combination between configuration interaction (CI) and HF.

Including additional possible determinants for excited electron configurations in the ground state improves the quality of the wave function. By selecting only a limited number of determinants from all possible, we can construct a multiconfigurational wave function, which can retrieve the static electron correlation energy. The most popular way to implement this is the Complete Active Space Self-Consistent Field (CASSCF) method.

CASSCF consists in the complete variational calculation of some electrons and some orbitals, in the average field of the rest of electrons in the rest of orbitals. It provides the static correlation energy and gives good quality potential energy surfaces, and hence it is also used as a starting point for higher-level multireference methods.

It has the advantage that it is applicable to excited states as well as the ground state and it provides size-consistent results. However, it often generates too many configurations, and therefore there is a problem in respect to how we could extract a chemical description from the lengthy CASSCF wave functions.

This method is convenient and overcomes many problems of HF calculations on open shell systems. However, it is difficult to recover a large portion of the dynamic correlation energy by expanding the active space. Its energies miss the effects of dynamic electron correlation.

The lowest-order of perturbation theory at which electron correlation effects arise is second-order. Given a reference wavefunction of the CASSCF type, second-order Multi-Reference Perturbation Theory (MRPT2) is already an elaborate undertaking. In this study we used the second-order N-Electron Valence Perturbation Theory (NEVPT2).

NEVPT2, upon forming excited CSFs does not excite each and every of them inside the CAS individually, but rather applies the excitation collectively to the entire CASSCF wavefunction.

The result of a NEVPT2 calculation is a second-order energy correction, ΔE^{PT2} , such that the total energy for each state is $E = E^{CAS} + \Delta E^{PT2}$. However, it is important to note that the wavefunction is not changed by the treatment and still remains a CASSCF wavefunction. Hence, all calculations are based on CASSCF wavefunctions in conjunction with second-order corrected total energies. It introduces the effects of dynamic electron correlation.

5.3. *AB INITIO* LIGAND FIELD THEORY (AILFT)

Ab initio methods are computational chemistry methods based on quantum chemistry, based on the determination of the wave function. That is why the term means “from first principles”. Their purpose is to solve the electronic Schrödinger equation given the positions of the nuclei and the number of electrons in the interest of provide information such as electron densities, energies and other properties of the system. Thus, this type of methods do not contain any type of experimental information.[7][8][11] The *Ab Initio* Ligand Field Theory method takes the complex results from NEVPT2 calculations and translate them to chemically meaningful crystal field parameters, which are easier to understand. Basically, provides the energy of the five d orbitals and the Racah parameters B and C.

5.4. ANGULAR OVERLAP MODEL (AOM)

The Angular Overlap Model (AOM) is a method of description of transition metal and ligand interactions and main group stereochemistry. Its basic assumption is that the strength of a bond formed using atomic orbitals on two atoms is related to the distance and the magnitude of overlap between the two orbitals.[10][14][15]

It is assumed that the total ligand field potential (V_{LF}) can be constructed as a sum of contributions from individual metal-ligand (M-L) bonds and that these contributions are localized. The complex can be treated as a set of diatomic molecules with the bonds divided into separate σ and π contributions which are modelled by AOM parameters such as e_σ, $e_{\pi x}$ and $e_{\pi y}$. That is to say, AOM parameterizes the M-L interactions based on the M-L distance and the position of the ligand around the metal using the parameters mentioned.

In AOM terms, the octahedral splitting Δ_{Oh} for ligands that only have σ contribution (typically amine ligands) is given by Equation 1.

$$\Delta_{Oh} = 3e_\sigma \qquad \text{Equation 1}$$

5.5. MOLECULAR MECHANICS/LIGAND-FIELD MOLECULAR MECHANICS (MM/LFMM)

Molecular mechanics (MM) computes the potential energy surface for a particular arrangement of atoms using potential functions that are derived using chemical physics. These equations are known as a force field. It is a methodology that parameterizes the potential with mathematical functions. With the temperature, we give initial speeds to the system and allow it to propagate following the Newton equations obtaining the energy and the forces of the system.[7][8]

This allows us to obtain a temporary evolution of the system in specific conditions, which can be, NVE (constant Number of particles, Volume and Energy), NVT (constant Number of particles, Volume and Temperature), NPT (constant Number of particles, Pressure and Temperature)/NσT (constant Number of particles, Stress tensor and Temperature), etc.

The advantage of MM is that it is extremely cheap from the computational point of view and allows to study large molecules (such as proteins).[7][8] The disadvantages are that is restricted by parameters of equations like different FF for different types of atoms (FF are not transferable) and it is not applicable for electronic properties (the potential energy surface corresponds to an electronic state).

In our case, a modified version of the MM is made which is the Ligand-Field Molecular Mechanics (LFMM) where the AOM is implemented within the molecular mechanics scheme.[14][16][17]

Summary of the procedure followed in this study:

This study focusses only on the low-spin Fe(II) system.

Performing DFT calculations, the Fe-N bond will be modelled using a Morse potential. This data will be adjusted simultaneously against an energy scan along the totally symmetric normal mode, in order to generate an *ab initio* force field for the molecule.

Also, a series of electronic structure calculations will be carried out at CASSCF/NEVPT2 level to extract the relevant AOM parameters for a very simple molecule, $[Fe(NH_3)_6]^{2+}$, representative (in principle) of the Fe(II) environment in $[Fe_4]$ MOCs; necessary to construct the force field.

After that, the construction and validation of the force field must be done. In order to see if the results of $[Fe(NH_3)_6]^{2+}$ can be extrapolated to a more complex systems like the $[Fe_4]$ cages, it will be verified if the approximation of the ammonia can be used in systems increasingly similar to the compound of study: $[Fe(py)_6]^{2+}$ and $[Fe(C_6H_6N_2)_3]^{2+}$. Then, the complete force field for the $[Fe_4]$ system will be assembled and tested.

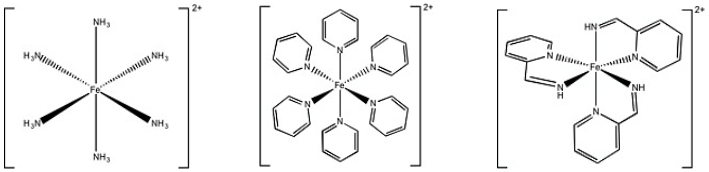

Figure 2. $[Fe(NH_3)_6]^{2+}$, $[Fe(py)_6]^{2+}$ and $[Fe(C_6H_6N_2)_3]^{2+}$, respectively.

Finally, LFMM simulations will be run in the NVE, NVT or NPT/NσT (it appears later in the study) ensemble to study the interaction between the $[Fe_4]$ system and the SF_6 molecule in a large enough system so the crystal packing effects can be properly modelled.

6. RESULTS

- All DFT calculations are performed with Gaussian09.[18]
- Arbitrary initial geometries are obtained using Gaussview.[19]
- All AILFT calculations are performed with ORCA4.0.[20]
- The program used to construct the FF is build_ff_lfm_morse4.f90.

- The programs used to validate the FF are DL-POLY-2.0 and Visual Molecular Dynamics (VMD).[21][22]
- The program used for the representation of the molecules and orbitals is VMD.[22]
- All graphics and fits in this study have been made using Gnuplot 4.6.[23]

6.1. $[Fe(NH_3)_6]^{2+}$

6.1.1. Geometry Optimization and calculation of Frequencies and NBO charges for $[Fe(NH_3)_6]^{2+}$ with DFT

The first step on this study is to obtain the optimized geometry of $[Fe(NH_3)_6]^{2+}$ (since it is a low-spin system, S=0).

In order to achieve that geometry, a structure of the complex is created with an arbitrary initial geometry using Gaussview, which is able to write the geometry in Cartesian coordinates. These coordinates are put then in a Gaussian input, in order to make a DFT calculation of optimization, frequencies and Natural Bond Orbital (NBO) charges using the hybrid meta-GGA TPSSh functional.[24] See Appendix 1 (Table A1.1 and Table A1.2) and Appendix 2 (Table A2.1).

Why do we need these data?

- The optimized geometry gives us information about the geometry that corresponds to the minimum of electronic energy and allows us to establish a range of distances to generate a local scan (study of the energy depending on the Fe-N bond distance), which is useful to determine e_σ values.
- Since all the frequencies are positive, we can assure that we are in a minimum of energy.
- NBO charges are more reliable than those given by Mulliken Population Analysis and will be useful later to construct the force field.

R_{eq}(Fe-N) = 2.08 Å

6.1.2. Local scan for $[Fe(NH_3)_6]^{2+}$ with DFT and AILFT

In order to study the dependence of energy on the Fe-N bond distance, a range of distances around the minimum has been chosen and the energy has been calculated on each of them: from 1.83 Å to 2.43 Å with 0.05Å increments. See Appendix 3 (Table A3.1).

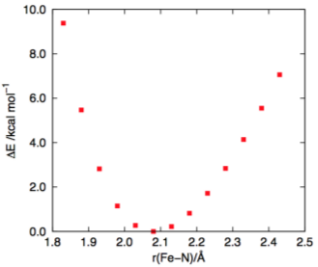

Figure 3. ΔE/kcal mol^{-1} vs r(Fe-N)/Å with DFT.

6.1.3. Sigma type bond parameter in AOM (e_σ) obtaining for $[Fe(NH_3)_6]^{2+}$: DFT vs AILFT

With the information of the local scan, it is possible to know which orbitals are occupied and which are virtual (unoccupied). In DFT method, the orbitals are chosen manually by looking the contribution coefficient of the molecular orbital at the d orbitals. It is obvious that this procedure will provide more error than a procedure that gives directly the d orbitals, as it does AILFT.

Then, it is possible to calculate Δ_{Oh} by subtracting the energy value of the less energetic virtual orbital by the energy value of the most energetic occupied orbital. Since $\Delta_{Oh}=3e_\sigma$, we can extract the e_σ value.

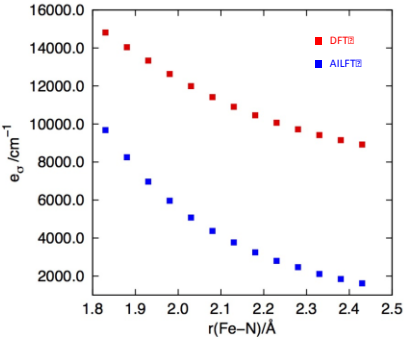

Figure 4. Dependence of e_σ on the Fe-N distance.

As we can see in the graphic, there is a big difference between the two methods. AILFT is more reliable than DFT because DFT does not provide a good description of the empty d orbitals, the energy of these virtual orbitals is not good enough due to methodological issues. By contrast, AILFT performs a huge analysis of different electronic possibilities by moving electrons from occupied orbitals to virtual orbitals providing all the possible excitations, which provides reliable energies. See Appendix 3 (Table A3.1) and Appendix 5 (Figure A5.1).

After this local scan, a fit of this M-L bond length dependence must be done in order to have a function that describes the d orbital splitting as a function of the bond distance, whereby we can calculate the ligand field splitting. This function describes the Fe-N sigma bond interaction. Together with the overlap factors, it is possible to calculate V_{LF}, which in turns allows us to compute the Ligand Field Stabilization Energy (LFSE).[14] From that energy term, it is possible to calculate more parameters related to the trajectory studies.

$$e_\sigma(r) = a_o + a_1 r + \frac{a_2}{r^2} + \frac{a_3}{r^3} + \frac{a_4}{r^4} + \frac{a_5}{r^5} + \frac{a_6}{r^6} \qquad \text{Equation 2}$$

Taking reference on Equation 2, we have tested three fits:

i. $e_\sigma = \frac{a_6}{r^6}$; $a_6 = 358843\ cm^{-1}\text{Å}^6$; error of 0.545%

ii. $e_\sigma = \frac{a_5}{r^5}$; $a_5 = 181743\ cm^{-1}\text{Å}^5$; error of 2.61%

iii. $e_\sigma = \frac{a_4}{r^4}$; $a_4 = 90489.1\ cm^{-1}\text{Å}^4$; error of 4.86%

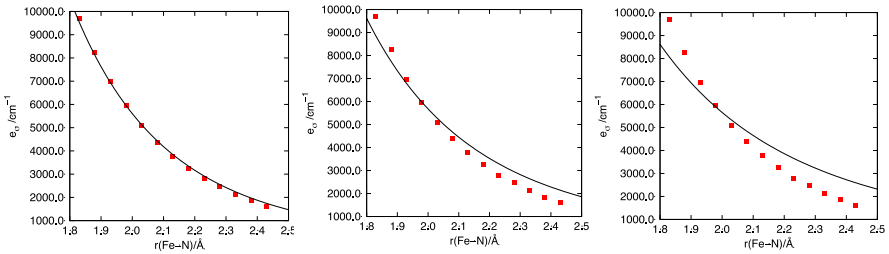

Figure 5. Fit of the bond length dependence on r^{-6}, r^{-5} and r^{-4} respectively.

Although it is clear that the best fit comes from r^{-6} dependence, the function chosen is the one that depends on r^{-4}. This will be discussed further in the FF construction.

6.1.4. Morse potential fit for $[Fe(NH_3)_6]^{2+}$ with DFT

In order to obtain a function that describes the Morse potential, it is required a scan of a large range of distances: starting with 1.8 Å, 64 steps with an increment of 0.05 Å, thus, from 1.8 Å to 5.0 Å. This scan is made using Gaussian09 at a DFT level.

To construct the FF, three parameters from the Morse potential are necessary: the dissociation energy, D_e, the equilibrium radium, R_{eq}, and the well width, α.

$$V(R) = D_e[(1 - e^{-\alpha(R-R_{eq})})^2 - 1] \qquad \text{Equation 3}$$

To calculate these parameters, the program Gnuplot needs initial values. We put, thus: D_e = 15 kcal mol^{-1}, R_{eq} = 2 Å and α = 2. Then, it has returned: D_e = 29.31 kcal mol^{-1} = 10251 cm^{-1} (error of 0.635%); R_{eq} = 2.10 Å (error of 0.216%); α = 1.47 (error of 1.231%). See Appendix 4 (Table A4.1).

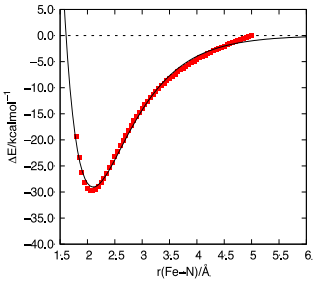

Figure 6. Morse potential fit for $[Fe(NH_3)_6]^{2+}$ per bond of Fe-N.

Now we have all the pieces to construct the force field.

6.1.5. Force Field Construction for $[Fe(NH_3)_6]^{2+}$

It will be easier to understand the construction of the FF by looking at the following scheme:

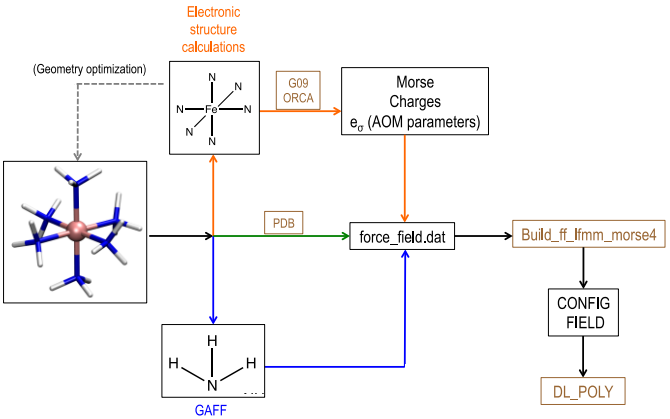

Figure 7. Process flow diagram.

First, it is necessary to create a pdb file with the optimized geometry of the molecule. Then, all the atoms must be labelled according to the Generalized Amber Force Field (GAFF) database.

GAFF atom type	**Atomic weight** [amu]	**Description**
fe	57.8450	There are no type of Fe
n4	14.0100	Sp3 N with four connected atoms
hn	1.0078	H bonded to nitrogen atoms

Table 1. Atom labels according to GAFF.

This pdb file is modified as a cubic cell of 500 Å × 500 Å × 500 Å with the molecule with its connectivity in the middle. In this way, all the information can be read and interpreted by the program build_ff_lfm_morse4, which will help us to construct the force field.

Once this is done, we create a file (force_field.dat) that contains all the parameters involved in the molecule by extracting information of the GAFF and of the electronic structure calculations performed before (charges, Morse and AOM parameters).

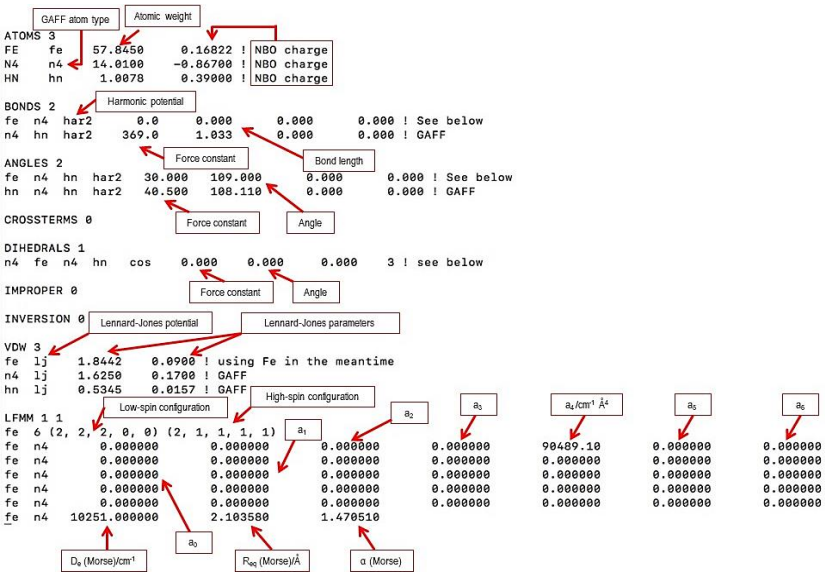


```
ATOMS 3
FE    fe      57.8450      0.16822 ! NBO charge
N4    n4      14.0100     -0.86700 ! NBO charge
HN    hn       1.0078      0.39000 ! NBO charge

BONDS 2
fe  n4  har2       0.0      0.000       0.000       0.000 ! See below
n4  hn  har2     369.0      1.033       0.000       0.000 ! GAFF

ANGLES 2
fe  n4  hn  har2   30.000   109.000      0.000       0.000 ! See below
hn  n4  hn  har2   40.500   108.110      0.000       0.000 ! GAFF

CROSSTERMS 0

DIHEDRALS 1
n4  fe  n4  hn   cos    0.000    0.000     0.000    3 ! see below

IMPROPER 0

INVERSION 0

VDW 3
fe  lj    1.8442    0.0900 ! using Fe in the meantime
n4  lj    1.6250    0.1700 ! GAFF
hn  lj    0.5345    0.0157 ! GAFF

LFMM 1 1
fe  6 (2, 2, 2, 0, 0) (2, 1, 1, 1, 1)
fe  n4        0.000000        0.000000        0.000000        0.000000        90489.10        0.000000        0.000000
fe  n4        0.000000        0.000000        0.000000        0.000000        0.000000        0.000000        0.000000
fe  n4        0.000000        0.000000        0.000000        0.000000        0.000000        0.000000        0.000000
fe  n4        0.000000        0.000000        0.000000        0.000000        0.000000        0.000000        0.000000
fe  n4        0.000000        0.000000        0.000000        0.000000        0.000000        0.000000        0.000000
fe  n4    10251.000000        2.103580        1.470510
```

Figure 8. force_field.dat file for $[Fe(NH_3)_6]^{2+}$.

We have to modify the input by putting the paths and the different parameters that requires and at the build_ff_lfmm_morse4.f90 we must check the distance cutoffs.

Then, we run the program and it returns the number of bonds, angles, dihedrals and Van Der Waals interactions. These data are set at the input file and the program is run again. Two files have been created, the FIELD (contains FF parameters) and the CONFIG (contains the initial Cartesian coordinates for the system).

Why do we use r^{-4} dependence?

We tried to run the trajectory with the dependence on r^{-6} and the calculation did not work. The same thing happened for r^{-5}. However, with the dependence on r^{-4} the calculation worked out, so we definitely chose this type of dependence. It is not the best fit, but it is still acceptable around the equilibrium bond length of 2 Å. There is not enough time to carry out an exhaustive methodological exploration. The time available to accomplish this study is limited.

In r^{-4}, small changes in the distance entail big changes in energy, but not as pronounced as in r^{-6}. Major changes in energy cause that small displacements will alter much the dynamics of the system. To avoid this, it is possible to change several parameters of the system (set a limit on the displacement of the atoms, modify the time step, etc.) so that we could use the function that depends on r^{-6}, which represents a better fit, but nevertheless it would take much time in testing which parameters are suitable. That is why we chose a function that does not lead to such big changes.

6.1.6. Force Field Validation for $[Fe(NH_3)_6]^{2+}$

The first step is to look for the potential well. We calculate a geometry optimization with the FF to test if it is close to the one calculated by the DFT method. Moreover, we have a starting structure at the potential well, therefore we avoid sudden changes that could end up with the calculation.

The second step is to run the trajectory at different temperatures in order to see the molecule's behaviour and to ensure if it is stable. The ensemble used is NVE.

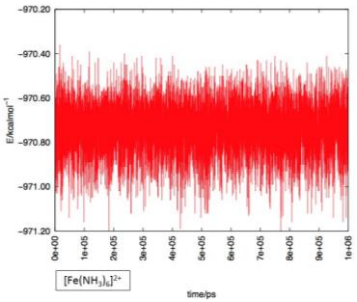

Figure 9. Energy dependence on time of $[Fe(NH_3)_6]^{2+}$ at 350 K.

6.2. $[Fe(py)_6]^{2+}$ AND $[Fe(C_6H_6N_2)_3]^{2+}$

The ligand of interest (the one from $[Fe_4]$ cages) has a nitrogen that is aromatic. To see if the calculations for the ammonia complex can be extrapolated, we will calculate the AOM parameters for a $[Fe(py)_6]^{2+}$ complex, which has an aromatic N, to find out if it has a different behaviour than the N of the ammonia. Then, we will also calculate the AOM parameters for a $[Fe(C_6H_6N_2)_3]^{2+}$ molecule (more similar to the ligand of interest) to see which type of nitrogen is better suited to the ligand; the ammonia type nitrogen, the pyridine nitrogen or both.

In other words, we assume that the possible π interactions that may exist due to the presence of aromatic N are negligible. This assumption will be validated below.

6.2.1. Geometry Optimization and calculation of Frequencies and NBO charges for $[Fe(py)_6]^{2+}$ and $[Fe(C_6H_6N_2)_3]^{2+}$ with DFT

The procedure is the same as the one followed in section 6.1.1 but for $[Fe(py)_6]^{2+}$ and $[Fe(C_6H_6N_2)_3]^{2+}$ systems. See Appendix 1 (Table A1.3, Table A1.4, Table A1.5 and Table A1.6) and Appendix 2 (Table A2.2 and Table A2.3) and Appendix 5 (Figure A5.2 and Figure A5.3).

- **$[Fe(py)_6]^{2+}$:** R_{eq}(Fe-N) = 2.09 Å
- **$[Fe(C_6H_6N_2)_3]^{2+}$:** R_{eq}(Fe-N) = 1.97 Å

6.2.2. Sigma type bond parameter in AOM (e_σ) obtaining for $[Fe(py)_6]^{2+}$ and $[Fe(C_6H_6N_2)_3]^{2+}$ with AILFT

As the calculation using AILFT returns better results than the one done with DFT, we calculate e_σ via AILFT at the equilibrium geometry. We do not perform a local scan yet; if the results of equilibrium geometry of pyridine and 2-picolylamine systems are similar to those of ammonia, and e_σ for pyridine and 2-picolylamine systems is close to the one given by the ammonia function, it will not be necessary to carry out a local scan.

Entry	r(Fe-N) [Å]	10Dq (AILFT) [cm^{-1}]	e_σ (AILFT) [cm^{-1}]
$[Fe(py)_6]^{2+}$	2.09	12416	4138.7
$[Fe(C_6H_6N_2)_3]^{2+}$	1.97	16772	5590.8

Table 2. 10Dq and e_σ values depending on the Fe-N bond length of $[Fe(py)_6]^{2+}$ and $[Fe(C_6H_6N_2)_3]^{2+}$.

6.2.3. $[Fe(py)_6]^{2+}$ and $[Fe(C_6H_6N_2)_3]^{2+}$ comparison to $[Fe(NH_3)_6]^{2+}$

To continue, we must compare the results of the ammonia system with the results of the pyridine and 2-picolylamine systems.

Entry	$[Fe(NH_3)_6]^{2+}$	$[Fe(py)_6]^{2+}$	$Fe(C_6H_6N_2)_3]^{2+}$
r(Fe-N) [Å]	2.08	2.09	1.97
10Dq (AILFT) [cm^{-1}]	13128	12416	16772
e_σ (AILFT) [cm^{-1}]	4376.1	4138.7	5590.8

Table 3. 10Dq and e_σ values depending on the Fe-N bond length of $[Fe(NH_3)_6]^{2+}$, $[Fe(py)_6]^{2+}$ and $[Fe(C_6H_6N_2)_3]^{2+}$.

Fit for $[Fe(NH_3)_6]^{2+}$ system: $e_\sigma = \frac{a_6}{r^6}$; $a_6 = 358843\ cm^{-1}\text{Å}^6$

- **$[Fe(NH_3)_6]^{2+}$:** $e_\sigma = \frac{358843\ cm^{-1}\text{Å}^6}{2.08^6\ \text{Å}^6} = 4431.2\ cm^{-1}$ close to 4376.1 cm^{-1}

- **$[Fe(py)_6]^{2+}$:** $e_\sigma = \frac{358843\ cm^{-1}\text{Å}^6}{2.09^6\ \text{Å}^6} = 4305.5\ cm^{-1}$ close to 4138.7 cm^{-1}

- **$[Fe(C_6H_6N_2)_3]^{2+}$:** $e_\sigma = \frac{358843\ cm^{-1}\text{Å}^6}{1.97^6\ \text{Å}^6} = 6139.1\ cm^{-1}$ close to 5590.8 cm^{-1}

e_σ for both pyridine and 2-picolylamine systems are close to the fit provided by the e_σ ammonia system.

Let's check if the fit is still good with an r^{-4} dependence:

Fit for $[Fe(NH_3)_6]^{2+}$ system: $e_\sigma = \frac{a_4}{r^4}$; $a_4 = 90489.1\ cm^{-1}\text{Å}^4$

- **$[Fe(NH_3)_6]^{2+}$:** $e_\sigma = \frac{90489.1\ cm^{-1}\text{Å}^4}{2.08^4\ \text{Å}^4} = 4834.4\ cm^{-1}$ close to 4376.1 cm^{-1}

- **$[Fe(py)_6]^{2+}$:** $e_\sigma = \frac{90489.1\ cm^{-1}\text{Å}^4}{2.09^4\ \text{Å}^4} = 4742.5\ cm^{-1}$ close to 4138.7 cm^{-1}

- **$[Fe(C_6H_6N_2)_3]^{2+}$:** $e_\sigma = \frac{90489.1\ cm^{-1}\text{Å}^4}{1.97^4\ \text{Å}^4} = 6008.0\ cm^{-1}$ close to 5590.8 cm^{-1}

We see that the results of the fit are close to those calculated for each complex. Therefore, we can simplify the metal-ligand interaction, the ammonia does reflect it properly. The results show that de nitrogen of the pyridine does not need to be treated in a different way than the nitrogen of the ammonia. Moreover, 2-picolylamine system fits properly with ammonia's e_σ function, which shows that both types of nitrogen can be treated equally. We do not provide much error neglecting the possible π interactions.

Thus, as previously said, it is not necessary to perform a local scan for $[Fe(py)_6]^{2+}$ to obtain a function that describes better the bond with the aromatic N, but we will. In this way we will fully demonstrate that we could take data from ammonia system, pyridine system or even both at the same time.

6.2.4. Local scan for $[Fe(py)_6]^{2+}$ with AILFT

A range of distances around the minimum has been chosen in order to study the dependence of energy on the Fe-N bond distance, and the energy has been calculated on each of them: from 1.84 Å to 2.44 Å with 0.05 Å increments.

6.2.5. Sigma type bond parameter in AOM (e_σ) obtaining for $[Fe(py)_6]^{2+}$

As explained in section 6.1.3, after the local scan, we perform a fit of this metal-ligand bond length dependence.

Taking reference on Equation 2, we have tested three fits:

i. $e_\sigma = \frac{a_6}{r^6}$; $a_6 = 354571\ cm^{-1}\text{Å}^6$; error of 0.999%

ii. $e_\sigma = \frac{a_5}{r^5}$; $a_5 = 178417\ cm^{-1}\text{Å}^5$; error of 3.07%

iii. $e_\sigma = \frac{a_4}{r^4}$; $a_4 = 88261.7\ cm^{-1}\text{Å}^4$; error of 5.32%

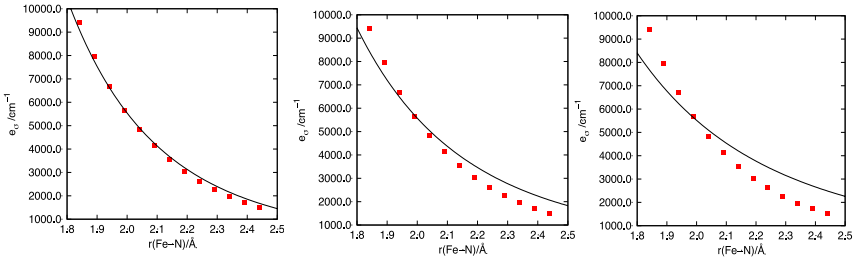

Figure 10. Fit of the bond length dependence on r^{-6}, r^{-5} and r^{-4} respectively.

The function chosen is the one that depends on r^{-4} for the same reason explained in section 6.1.5.

We see that the values of a_6, a_5, and a_4 obtained for the pyridine complex are quite similar to those obtained by the ammonia system (section 6.1.3). Therefore, an ammonia type nitrogen and a pyridine type nitrogen can be treated in the same way. See Appendix 3 (Table A3.2).

6.2.6. Morse potential fit for $[Fe(py)_6]^{2+}$ with DFT

As said in section 6.1.4, in order to obtain a function that describes the Morse potential, it is required a scan of a large range of distances: from 1.8 Å to 5.0 Å.

In order to construct the FF, three parameters from the Morse potential are necessary: D_e, R_{eq}, and α (see Equation 3). To calculate these parameters, we put as initial values: D_e = 15 kcal mol^{-1}, R_{eq} = 2 Å and α = 2. Then, the program has returned: D_e = 24.25 kcal mol^{-1} = 8481.8 cm^{-1} (error of 0.534%), R_{eq} = 2.36 Å (error of 0.122%), α = 1.42 (error of 0.566%). See Appendix 4 (Table A4.2).

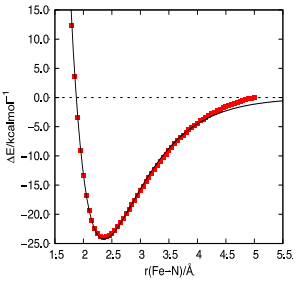

Figure 11. Morse potential fit for $[Fe(py)_6]^{2+}$ per bond of Fe-N.

We see that the values of D_e, R_{eq} and α obtained for the pyridine complex are quite similar to those obtained by the ammonia system (section 6.1.4). Therefore, both type of N can be treated equally.

6.3. $[Fe_4]$ CAGE SYSTEM

6.3.1. μ²-4,4'-bis([(pyridin-2-yl)methylidene]amino)biphenyl-2,2'-disulfonate ligand

6.3.1.1. Calculation of NBO charges for [Fe4] empty cage system

The first step is to download the pdb file that has de $[Fe_4]$ cage system without the counter ions and the guest molecule.[25]

As it is a complex system, we tried to assemble a FF with the charges provided by GAFF, but for a repulsion issue it did not work, so we decided to calculate the NBO charges. Of the whole system, we only keep the ligand so the calculation will be easier and faster.

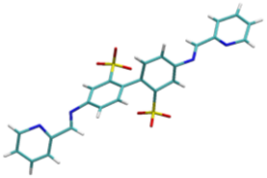

Figure 12. Molecular representation of the μ^2-4,4'-bis([(pyridin-2-yl)methylidene]amino)biphenyl-2,2'-disulfonate ligand.[25]

Each type of atom has different charges, so we calculate an average of these. Then, we have to compare these charges with those (also average) obtained for the $[Fe(py)_6]^{2+}$ and $[Fe(C_6H_6N_2)_3]^{2+}$ systems since they contain similar type of nitrogen involved in the ligand, and then, decide which charges choose for the FF construction. See Appendix 2 (Table A2.2, Table A2.3 and Table A2.4).

GAFF atom type	Atomic weight [amu]	Description	GAFF atom type	Atomic weight [amu]	Description
fe	57.845	There are no type of Fe	hc	1.008	H bonded to aliphatic carbon without electrowithdrawing group
ca	12.010	Sp2 C in pure aromatic systems	nb	14.010	Sp2 N in pure aromatic systems
ce	12.010	Inner Sp2 carbons in conjugated systems	ne	14.010	Inner Sp2 N in conjugated systems
cp	12.010	Head Sp2 C that connect two rings in biphenyl systems	s6	32.06	S with four connected atoms
ha	1.008	H bonded to aromatic carbon	o	16.00	Oxygen with one connected atom

Table 4. Atom labels of the ligand according to GAFF.

GAFF atom type	Atomic weight [amu]	Description	GAFF atom type	Atomic weight [amu]	Description
fe	57.845	There are no type of Fe	hc	1.008	H bonded to aliphatic carbon without electrowithdrawing group
ca	12.010	Sp2 C in pure aromatic systems	hn	1.008	H bonded to nitrogen atoms
ce	12.010	Inner Sp2 carbons in conjugated systems	nb	14.010	Sp2 N in pure aromatic systems
ha	1.008	H bonded to aromatic carbon	ne	14.010	Inner Sp2 N in conjugated systems

Table 5. Atom labels of $[Fe(C_6H_6N_2)_3]^{2+}$ according to GAFF.

GAFF atom type	Atomic weight [amu]	Description	GAFF atom type	Atomic weight [amu]	Description
fe	57.845	There are no type of Fe	ha	1.008	H bonded to aromatic carbon
ca	12.010	Sp2 C in pure aromatic systems	nb	14.010	Sp2 N in pure aromatic systems

Table 6. Atom labels of $[Fe(py)_6]^{2+}$ according to GAFF.

Considering that [Fe_4] empty cage system and [$Fe(C_6H_6N_2)_3]^{2+}$ have more types of atoms in common than [Fe_4] empty cage system and [$Fe(py)_6]^{2+}$ systems (see Table 4, Table 5 and Table 6), we have opted for the NBO charges of [Fe_4] empty cage system and [$Fe(C_6H_6N_2)_3]^{2+}$.

Entry	Charges from [Fe_4] empty cage	Charges from [$Fe(C_6H_6N_2)_3]^{2+}$	Entry	Charges from [Fe_4] empty cage	Charges from [$Fe(C_6H_6N_2)_3]^{2+}$
fe	-	-0.03500	cp	-0.03400	-
nb	-	-0.28633	ha	-	0.23942
ne	-	-0.43033	hc	-	0.22333
ca	-	-0.06307	s6	2.31050	-
ce	-	0.13200	o	-0.98117	-

Table 7. NBO charges chosen for the FF construction.

6.3.1.2. Force Field Construction and Validation for [Fe_4] empty cage system

The steps are similar to those of section 6.1.5 but for [Fe_4] empty cage system.

As the parameters obtained by both the ammonia complex and the pyridine complex are quite similar, it will be possible to use only data from one N type atom. However, we will use both, taking advantage of the fact that we have made the calculations for both N types.

LIGAND-FIELD MOLECULAR MECHANICS (LFFM):

AOM parameters:

- fe nb: a_4 from $[Fe(py)_6]^{2+}$ which is 88261.7 $cm^{-1}Å^4$
- fe ne: a_4 from $[Fe(NH_3)_6]^{2+}$ which is 90489.1 $cm^{-1}Å^4$

Morse parameters:

- fe nb: from $[Fe(py)_6]^{2+}$ which are D_e = 8481.8 cm^{-1}; R_{eq} = 2.36 Å; α = 1.42
- fe ne: from $[Fe(NH_3)_6]^{2+}$ which are D_e = 10251 cm^{-1}; R_{eq} = 2.10 Å; α = 1.47

The steps to validate the FF are the same as those in section 6.1.6 but for [Fe_4] empty cage system. The ensemble used is NVE.

When we check the trajectory, we see that the calculation does not work and several angles of the system are not as they should. We think that the problem comes from a charges issue. Thus, we modify a little bit the s6 atom charge, which finally has a value of 1.97193, so that the global charge of the system is -4 approximately.

When we check the trajectory again, we see that the calculation does not work either. We have discovered that the problem comes from the ensemble used. If we use a NVE ensemble, the calculation does not work, but if we use a NVT or NPT/NσT ensemble, it does. Thus, we change it. See Figure 1 (Left).

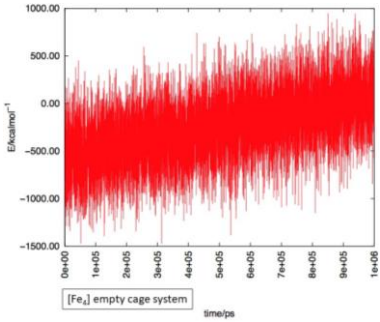

Figure 13. Energy dependence on time of [Fe_4] empty cage system at 300 K.

6.3.2. Counter ion $[N(CH_3)_4]^+$

It is necessary to introduce counter ions to the system, which is negatively charged. Thus, the geometry optimization with DFT, and the construction of the FF for tetramethylammonium cation must be done.

6.3.2.1. Geometry Optimization and calculation of Frequencies and NBO charges for $[N(CH_3)_4]^+$ with DFT

The procedure is the same as the one followed in section 6.1.1 but for $[N(CH_3)_4]^+$ cation. See Appendix 1 (Table A1.7 and Table A1.8) and Appendix 2 (Table A2.5)

R_{eq}(N-C) = 1.51 Å

6.3.2.2. Force Field Construction and Validation for $[N(CH_3)_4]^+$

The steps are the same than those of section 6.1.5 and 6.1.6 but with the tetramethylammonium cation. The ensemble used is NVE.

GAFF atom type	**Atomic weight** [amu]	Description
c3	12.0100	Sp3 C
n4	14.0100	Sp3 N with four connected atoms
h1	1.0080	H bonded to aliphatic carbon with 1 electrowithdrawing group

Table 8. Atom labels of $[N(CH_3)_4]^+$ cation according to GAFF.

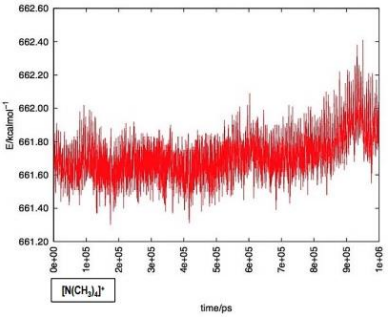

Figure 14. Energy dependence on time of $[N(CH_3)_4]^+$ at 300 K.

6.3.3. Guest molecule SF_6

Now we have to construct the FF for the guest molecule SF_6 and then, with all the pieces, construct the FF for the $[Fe_4]$ cage system.

6.3.3.1. Geometry Optimization and calculation of Frequencies and NBO charges for SF_6 with DFT

The procedure is the same as the one followed in section 6.1.1 but for SF_6 molecule. See Appendix 1 (Table A1.9 and Table A1.10) and Appendix 2 (Table A2.6).

R_{eq}(S-F) = 1.61 Å

6.3.3.2. Morse potential fit for SF_6 with DFT

It would not be necessary to perform a Morse potential fit if the GAFF had the harmonic potential parameters for the S and the F. As GAFF does not have the necessary parameters for our type of S and F, we must enter the parameters of the Morse potential.

As said in section 6.1.4, in order to obtain a function that describes the Morse potential, it is required a scan of a large range of distances: starting with 1.3 Å, 100 steps with an increment of 0.05 Å, thus, from 1.3 Å to 6.3 Å.

Initial values: D_e = 100 kcal mol^{-1}, R_{eq} = 2 Å and α = 1.5. Then, the program returns: D_e = 107.405 kcal mol^{-1} = 37565 cm^{-1} (error of 0.476%); R_{eq} = 1.63479 Å (error of 0.120%); α = 1.76186 (error of 0.596%). See Appendix 4 (Table A4.3).

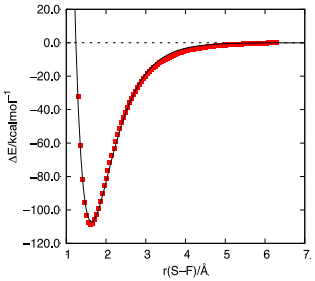

Figure 15. Morse potential fit for SF_6 per bond of S-F.

6.3.3.3. Force Field Construction and Validation for SF_6

The steps are the same than those of section 6.1.5 and 6.1.6 but for SF_6 molecule.

In the GAFF force field there are no standard parameters for this type of F and S atoms. Therefore, we had to define three different type of F. If not, the geometry of the molecule is not octahedral because the angles are not well defined. Thus, we label them as f1, f2, f3 and s.

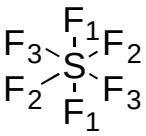

Figure 16. SF_6 with the different type of F.

GAFF atom type	Atomic weight [amu]
s	32.06
f1	19.00
f2	19.00
f3	19.00

Table 9. Atom labels (not GAFF).

The file force_field.dat contains all the parameters involved in the molecule by extracting information of the Morse potential (D_e, α and R_{eq}), of the GAFF force field (Van Der Waals parameters and force constant of the angles) and of the electronic structure calculations performed.

The ensemble used is NVE.

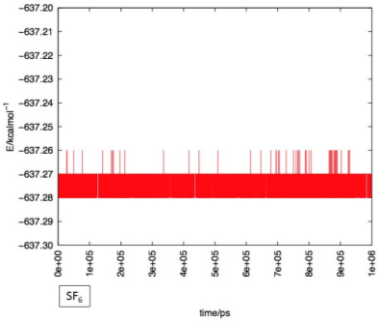

Figure 17. Energy dependence on time of SF_6 at 300 K.

6.3.4. Force Field Construction and Validation for the global [Fe_4] cage system

Once we have all the pieces, we can construct the global FF of study. The steps are the same than those explained at the previous FF constructions but with the addition of all the pieces to the calculation.

The parameters to construct this FF are the same used in the previous FF for each piece of the system. We pick the same final values used for $[N(CH_3)_4]^+$, SF_6 and [Fe_4] empty cage.

First, we test the FF in the NVT ensemble at different temperatures, and then we do the same in the NPT and NσT ensembles. See Figure 1 (Right).

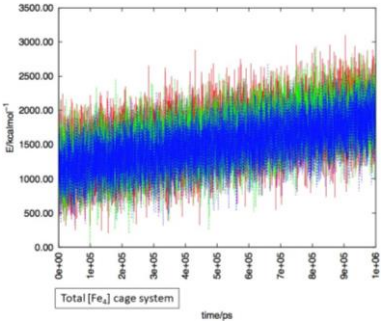

Figure 18. Energy dependence on time of [Fe4] cage system at 100 K (blue), 200 K (green) and 300 K (red).

7. DISCUSSION

7.1. GEOMETRY OPTIMIZATION AND CALCULATION OF FREQUENCIES AND NBO CHARGES FOR $[Fe(NH_3)_6]^{2+}$, $[Fe(py)_6]^{2+}$, $[N(CH_3)_4]^{+}$ AND SF_6

See Appendix 1. The results show an octahedral optimized geometry for $[Fe(NH_3)_6]^{2+}$, $[Fe(py)_6]^{2+}$, $[Fe(C_6H_6N_2)_3]^{2+}$ and SF_6 as expected, with a Fe-N bond length of 2.08 Å, 2.09 Å and 1.97 Å respectively for the nitrogen complexes, and a S-F bond length of 1.61 Å for SF_6.

The results show a tetrahedral optimized geometry for $[N(CH_3)_4]^{+}$ as expected, with a N-C bond length of 1.51 Å.

See Appendix 1. All frequencies are positive in each compound; hence, we can assure that we are in a minimum of energy.

See Appendix 2. NBO charges are useful to construct the FF and are more reliable than Mulliken charges since they operate on the electron density instead. Thus, polarization of bonds is considered. NBO describes better the Lewis-type molecular bonding pattern of electronic pairs. The population analysis of Mulliken shares the total electronic density between the atoms of the

molecule. The distribution of charges obtained by Mulliken is arbitrary and should be taken with a certain caution, since in some cases erroneous charge distributions may occur, inconsistent with the dipole moment of the system. One of the problems that has been observed with Mulliken's charges is that they are strongly dependent on the basis set and the description becomes worse by increasing it.

7.2. LOCAL SCAN FOR $[Fe(NH_3)_6]^{2+}$ AND $[Fe(py)_6]^{2+}$

See Figure 3 and Appendix 3. If we consider only the Fe-N bond (as a system formed by two atoms), initially they are so separated that they do not exert any influence on each other. As Fe and N start approximating each other, the attractive forces (long-range) of one of the nucleus over the electronic cloud of the other (V_{Ne}) begin to be noticed and vice versa. This stabilizes the system; therefore, the energy of the system decreases to a valley of minimum energy. However, as Fe and N keep getting closer, the repulsive (short-range) forces of one electronic cloud over the other (V_{ee}) start to be noticed, which destabilizes the system and cause the increase of the energy.

7.3. SIGMA TYPE BOND PARAMETER IN AOM (e_σ) OBTAINING FOR $[Fe(NH_3)_6]^{2+}$ (DFT VS AILFT), $[Fe(py)_6]^{2+}$ AND $[Fe(C_6H_6N_2)_3]^{2+}$

See Figure 4, Figure 5, Figure 10 and Appendix 3 (Table A3.1 and Table A3.2).

Part of these results (choice of the fitting parameters and debate between DFT and AILFT) are discussed in sections 6.1.3 and 6.1.5.

As Fe-N bond length increases, e_σ decreases. t_{2g} orbitals in these kinds of complexes have a non-bonding nature and the e_g orbitals have an antibonding nature. In the ideal case, increasing of the M-L distance causes the stabilization of the antibonding orbitals (decrease of energy) as the interaction between atoms is lower.

The discussion about the different type of N and their e_σ values is in sections 6.2.3 and 6.2.5.

7.4. MORSE POTENTIAL FIT FOR $[Fe(NH_3)_6]^{2+}$, $[Fe(py)_6]^{2+}$, $[N(CH_3)_4]^+$ AND SF_6

See Figure 6, Figure 11, Figure 15 and Appendix 4 (Table A4.1, Table A4.2 and Table A4.3).

The explanation of the behaviour of the energy depending on the bond length is the same that those explained in section 7.2.

If we look at Equation 3 we can see that when $R<R_{eq}$, the function tends to $+\infty$, and when $R>R_{eq}$, the function tends to zero.

The discussion about the different type of N and their values of the Morse parameters is in section 6.2.6.

7.5. $[Fe(NH_3)_6]^{2+}$ $[Fe(py)_6]^{2+}$ AND $[Fe(C_6H_6N_2)_3]^{2+}$ BEHAVIOUR

If we look at the following table, we can see that the ammonia N and the pyridine N have nearly the same values in the fits performed, which means that are similar.

Compound	Fit of Fe-N bond length dependence			Morse parameters			Sigma type bond parameter in AOM e_σ [cm^{-1}]
	a_6 [cm^{-1} Å^6]	a_5 [cm^{-1} Å^5]	a_4 [cm^{-1} Å^4]	D_e [kcal mol^{-1}]	R_{eq} [Å]	α	
$[Fe(NH_3)_6]^{2+}$	358843	181743	90489.1	29.31	2.10	1.47	4376.1
$[Fe(py)_6]^{2+}$	354571	178417	88261.7	24.25	2.36	1.42	4138.7
$[Fe(C_6H_6N_2)_3]^{2+}$	-	-	-	-	-	-	5590.8

Table 10. Comparison table of each complex.

In addition, the results obtained from e_σ ($\Delta_{Oh}/3$) are as expected according to the spectrochemical series of the ligands for an octahedral crystal field, in which the ligands are arranged in order of increasing energy of transitions that occur when they are present in a complex:[26]

Δ_{Oh}: $I^- < Br^- < S^{2-} <$ **S**$CN^- < Cl^- <$ N**O**$_2^- < N^{3-} < F^- < OH^- < C_2O_4^{2-} < O^{2-} < H_2O <$ **N**$CS^- < CH_3C{\equiv}N <$ py $<$ $NH_3 <$ en $<$ bpy $<$ phen $<$ **N**$O_2^- < PPh_3 <$ **C**$N^- <$ CO

py: pyridine; en: ethylenediamine; bpy: bipyridine; phen: phenanthroline; PPh_3: triphenylphosphine

Pyridine is a ligand that has a weaker field than NH_3, but not much. According to the results, 2-picolylamine is the strongest field ligand in this study.

7.6. Force Field Construction and Validation for $[Fe(NH_3)_6]^{2+}$, $[Fe_4]$ empty cage system, $[N(CH_3)_4]^+$, SF_6 and $[Fe_4]$ cage system

See Figure 9, Figure 13, Figure 14, Figure 17 and Figure 18.

As we can see in the graphic, the dependence of the total energy of the system over time is quite stable, no sudden changes are observed. This indicates that the FF created is stable. If we look at the $[Fe_4]$ cages total system, we see that the three trajectories (100 K, 200 K and 300 K) are practically identical, the only thing that changes is the fluctuation due to the temperature. The higher the temperature, the more oscillations in the energy, as expected.

The most stable molecule over the time is SF_6 because it is a closed shells system. Tetramethylamonium cation is a closed shells system too, but it is positively charged, it is more flexible, and the methyl groups have rotation. That is why it does not have a stability as clearly defined as SF_6.

When we look at the trajectory with the VMD, it is observed that the SF_6 is confined inside the cage and tends to get close to the vertices of the tetrahedron formed by the macromolecule. We should set up a program that at each step of the simulation would measure the Fe-S distance and return us where the molecule has been. Normally, it is done with a radial distribution function, which is a measure of the probability of finding a particle at a certain distance away from a given reference particle.[27] Anyway, this behaviour could be explained due to electrostatic interactions between Fe(II) and F that have a certain negative charge density.

7.7. Choice of the ensemble

DL_POLY allows to test FF with net charge. The NVE ensemble is the most comfortable to see if everything works. Therefore, testing of the FF for the different parts of the system are made with NVE.

Then, we must use ensembles that describe better the reality of the system once it has all its parts. We start with NVT and then with NPT/NσT (NPT and NσT are equivalent, the difference is that in NPT the pressure is isotropic and in NσT it is anisotropic). NσT is a more realistic description of the system because it allows the system to deform.

8. CONCLUSIONS

- The results of the calculations for the three model complexes containing Fe-N bonds produce similar results for the ligand field around the metal centre.
- Fe-N bonds on [Fe_4] cages can be described using a simple model such as $[Fe(NH_3)_6]^{2+}$. $[Fe(py)_6]^{2+}$ can also be used but becomes more expensive from the computational point of view due to its size. In any case, the N atoms in both ammonia and pyridine are similar in terms of bonding, and have a comparable behaviour to the N atom in the [Fe_4] cage system.
- Using AILFT, the relative position of ammonia, pyridine and 2-picolylamine in the spectrochemical series has been determined. As expected, pyridine has a slighter weaker ligand field than ammonia, and 2-picolylamine has the strongest ligand field in the study: $\Delta_{Oh}([Fe(NH_3)_6]^{2+})$=13128 cm^{-1}; $\Delta_{Oh}([Fe(py)_6]^{2+})$=12416 cm^{-1}; $\Delta_{Oh}([Fe(C_6H_6N_2)_3]^{2+})$=16772 cm^{-1}.
- All constructed force fields are stable and provide a reasonable representation of the potential energy surface for the [Fe_4] cages.
- SF_6 is confined inside the [Fe_4] cage and tends to get close to the vertices of the tetrahedron formed by the macromolecule due to electrostatic interactions between Fe(II) and F that have a certain negative charge density.

9. REFERENCES AND NOTES

[1] L. (VCH) VonJ.-M., *Supramolecular Chemistry. Concepts and Perspectives.*, vol. 107, no. 21. 1995.

[2] I. A. Riddell, M. M. J. Smulders, J. K. Clegg, and J. R. Nitschke, "Encapsulation, storage and controlled release of sulfur hexafluoride from a metal-organic capsule," *Chem. Commun.*, 2011.

[3] A. M. Rosan, "Green Chemistry: An Introductory Text (Lancaster, Mike)," *J. Chem. Educ.*, vol. 80, no. 10, p. 1141, Dec. 2009.

[4] M. A. Halcrow, *Spin-Crossover Materials: Properties and Applications*. John Wiley and Sons, 2013.

[5] R. A. Bilbeisi *et al.*, "Guest binding subtly influences spin crossover in an FeII4L4 capsule," *Chem. - A Eur. J.*, vol. 19, no. 25, pp. 8058–8062, 2013.

[6] J. Cirera, V. Babin, and F. Paesani, "Inorg. Chem. 2014, 53, 11020–11028, Theoretical Modeling of Spin Crossover in Metal−Organic Frameworks [Fe(pz)2Pt(CN)4] as a Case Study.pdf," 2014.

[7] C. J. Cramer, *Essentials of Computational Chemistry Theories and Models*. 2004.

[8] F. Jensen, *Introduction to Computational Chemistry*. 2014.

[9] J. Wang, R. M. Wolf, J. W. Caldwell, P. A. Kollman, and D. A. Case, "Junmei Wang, Romain M. Wolf, James W. Caldwell, Peter A. Kollman, and David A. Case, 'Development and testing of a general amber force field'Journal of Computational Chemistry(2004) 25(9) 1157-1174," *J. Comput. Chem.*, vol. 26, no. 1, pp. 114–114, Jan. 2005.

[10] C. E. Schäffer and C. K. Jørgensen, "The angular overlap model, an attempt to revive the ligand field approaches," *Mol. Phys.*, vol. 9, no. 5, pp. 401–412, Jan. 1965.

[11] S. K. Singh, J. Eng, M. Atanasov, and F. Neese, "Covalency and chemical bonding in transition metal complexes: An ab initio based ligand field perspective," *Coord. Chem. Rev.*, vol. 344, pp. 2–25, 2017.

[12] E. I. Solomon *et al.*, "Copper Active Sites in Biology," *Chem. Rev.*, vol. 114, no. 7, pp. 3659–3853, Apr. 2014.

[13] S. Edition, W. Koch, and M. C. Holthausen, "Wolfram Koch , Max C . Holthausen A Chemist ' s Guide to," *Neural Networks*, vol. 3, p. 294, 2001.

[14] R. J. Deeth, A. Anastasi, C. Diedrich, and K. Randell, "Molecular modelling for transition metal complexes: Dealing with d-electron effects," *Coord. Chem. Rev.*, vol. 253, no. 5–6, pp. 795–816, 2009.

[15] "angular overlap model (AOM)," *IUPAC Compendium of Chemical Terminology*. [Online]. Available: http://goldbook.iupac.org/AT06986.html. [Accessed: 06-Jun-2019].

[16] R. Deeth, "The ligand field molecular mechanics model and the stereoelectronic effects of d and s electrons," *Coord. Chem. Rev.*, vol. 212, no. 1, pp. 11–34, Feb. 2001.

[17] R. J. Deeth, N. Fey, and B. Williams–Hubbard, "DommiMOE: An implementation of ligand field molecular mechanics in the molecular operating environment," *J. Comput. Chem.*, vol. 26, no. 2, pp. 123–130, Jan. 2005.

[18] M. J. Frisch *et al.*, "Gaussian09," *Journal of the American Statistical Association*. 2009.

[19] R. Dennington, T. Keith, and J. Millam, "Gaussview, Version 5.," *Semichem Inc. , Shawnee Mission, KS*. p. Semichem Inc, 2016.

[20] F. Neese, "Software update: the ORCA program system, version 4.0," *Wiley Interdiscip. Rev. Comput. Mol. Sci.*, vol. 8, no. 1, 2018.

[21] W. Smith and T. R. Forester, "DL-POLY-2.0: A general-purpose parallel molecular dynamics

simulation package," *J. Mol. Graph.*, vol. 14, no. 3, pp. 136–141, Jun. 1996.
[22] W. Humphrey, A. Dalke, and K. Schulten, "VMD: Visual molecular dynamics," *J. Mol. Graph.*, 1996.
[23] T. Williams *et al.*, "Gnuplot 4.6," *Softw. Man.*, 2014.
[24] V. N. Staroverov, G. E. Scuseria, J. Tao, and J. P. Perdew, "Comparative assessment of a new nonempirical density functional: Molecules and hydrogen-bonded complexes," *J. Chem. Phys.*, vol. 119, no. 23, pp. 12129–12137, Dec. 2003.
[25] C. R. Groom, I. J. Bruno, M. P. Lightfoot, and S. C. Ward, "The Cambridge Structural Database.," *Acta Crystallogr. B. Struct. Sci. Cryst. Eng. Mater.*, 2016.
[26] P. W. Atkins, T. Overton, J. Rourke, M. Weller, F. Armstrong, and M. Hagerman, *Shriver & Atkins' Inorganic Chemistry*. Oxford University Press, 2010.
[27] D. Frenkel and B. Smit, *Understanding Molecular Simulation: From Algorithms to Applications*. Academic Press, 2002.

10. ACRONYMS

- AILFT: *Ab Initio* Ligand Field Theory
- AOM: Angular Overlap Model
- CASSCF: Complete Active Space Self-Consistent Field
- CHARMM: Chemistry at Harvard Macromolecular Mechanics
- CI: configuration interaction
- CSFs: configuration state functions
- DFT: Density Functional Theory
- FF: force field
- GAFF: Generalized Amber Force Field
- HF: Hartree-Fock
- LFMM: Ligand-Field Molecular Mechanics
- LFSE: Ligand Field Stabilization Energy
- MCSF: Multi-Configurational Self-Consistent Field
- meta-GGA TPSSh: hybrid meta-Generalized Gradient Approximation Tao-Perdew-Staroverov-Scuseria
- M-L: metal-ligand
- MM: molecular mechanics
- MOCs: metal-organic cages
- MRPT2: second-order Multi-Reference Perturbation Theory
- NBO: Natural Bond Orbital
- NEVPT2: second-order N-Electron Valence Perturbation Theory
- NPT: constant Number of particles, Pressure and Temperature
- NσT: constant Number of particles, Stress tensor and Temperature
- NVE: constant Number of particles, Volume and Energy
- NVT: constant Number of particles, Volume and Temperature
- SCO: spin-crossover
- V_{LF}: ligand field potential
- VMD: Visual Molecular Dynamics

APPENDICES

APPENDIX 1: OPTIMIZED GEOMETRY IN CARTESIAN COORDINATES, LOWEST FREQUENCY AND ENERGY OF THE MINIMUM (DFT)

$[Fe(NH_3)_6]^{2+}$

Atom	Coordinates [Å]			Atom	Coordinates [Å]		
	x	y	z		x	y	z
Fe	0.00045	-0.000682	0.000731	N	2.083174	-0.001422	-0.022745
N	0.03684	2.081443	0.039496	H	2.508603	-0.896665	-0.271257
H	0.706348	2.462942	0.710578	H	2.481605	0.660259	-0.691751
H	0.292457	2.52655	-0.844107	N	-0.020779	-0.000865	-2.081923
N	-0.014706	-0.037136	2.083151	H	-0.705989	-0.645269	-2.481138
H	-0.679724	-0.708066	2.47269	H	-0.24711	0.897684	-2.512723
H	0.874649	-0.290698	2.517845	H	-0.850441	2.520692	0.292468
N	-2.081992	0.036743	-0.012604	H	2.525939	0.247536	0.863938
H	-2.471376	0.719727	-0.665338	H	0.862636	-0.271332	-2.518534
H	-2.528319	-0.842688	-0.280204	H	-0.888229	-2.515134	0.262528
N	-0.000177	-2.083486	-0.000646	H	-0.264501	0.849712	2.525084
H	0.228617	-2.511803	-0.899746	H	-2.512246	0.272208	0.883847
H	0.67427	-2.490252	0.650362				

Table A1.1. Optimized geometry of $[Fe(NH_3)_6]^{2+}$.

Lowest Frequency [cm^{-1}]	Minimum Energy [a.u]
50.08	-1602.850364

Table A1.2. Lowest frequency and minimum energy of $[Fe(NH_3)_6]^{2+}$.

$[Fe(py)_6]^{2+}$

Atom	Coordinates [Å]			Atom	Coordinates [Å]			Atom	Coordinates [Å]		
	x	y	z		x	y	z		x	y	z
Fe	0.211968	0.292062	-0.000157	C	-3.949759	-0.75725	-0.510224	H	-1.844875	0.672939	-2.283755
C	-0.446197	3.084311	-0.932474	H	-1.995222	-1.51899	-0.965189	C	0.159716	0.301807	-4.96761
C	0.878313	3.079287	0.941794	C	-3.934523	1.353591	0.599584	H	2.277764	-0.079637	-4.76626
C	-0.466141	4.470567	-0.967385	H	-1.968291	2.109653	1.011494	H	-1.953647	0.682202	-4.720269
H	-0.980788	2.519862	-1.679496	C	-4.658167	0.299199	0.052573	H	0.148338	0.304005	-6.050966
C	0.902252	4.465358	0.981332	H	-4.457953	-1.604842	-0.953098	C	2.983822	-0.731155	0.507857
H	1.411216	2.510864	1.686999	H	-4.430392	2.202598	1.05358	C	2.975856	1.306907	-0.565102
C	0.219099	5.185599	0.008164	H	-5.74162	0.300727	0.064527	C	4.370167	-0.771545	0.508387
H	-1.016709	4.972753	-1.753157	C	0.849702	-2.496624	-0.957302	H	2.413059	-1.529011	0.959367
H	1.454224	4.963326	1.768801	C	-0.43322	-2.499084	0.945714	C	4.36201	1.343087	-0.594252
H	0.220655	6.269057	0.00997	C	0.869138	-3.882734	-0.997929	H	2.398342	2.106508	-1.004774
C	1.366221	0.489707	2.848797	H	1.367534	-1.929108	-1.713749	C	5.082117	0.28467	-0.050346
C	-0.882877	0.083596	2.871269	C	-0.455923	-3.885305	0.980555	H	4.87552	-1.622137	0.948748
C	1.42483	0.492367	4.234833	H	-0.94972	-1.933523	1.70453	H	4.860739	2.192142	-1.045013
H	2.269221	0.660351	2.285173	C	0.205762	-4.601631	-0.010187	H	6.165578	0.282998	-0.06156
C	-0.912831	0.075842	4.258203	H	1.402297	-4.381819	-1.797562	N	0.215056	2.367458	0.003462
H	-1.797269	-0.085267	2.325783	H	-0.990253	-4.386467	1.778105	N	0.234189	0.288033	2.134974
C	0.26344	0.2828	4.967239	H	0.204478	-5.685092	-0.012454	N	2.267262	0.288947	-0.021278
H	2.377548	0.660253	4.721718	C	1.306025	0.092473	-2.872628	N	0.18946	0.296106	-2.135371
H	-1.855271	-0.093975	4.764053	C	-0.942333	0.502583	-2.84819	N	-1.843346	0.295184	0.021527
H	0.274638	0.280804	6.0506	C	1.335733	0.089979	-4.259588	N	0.20906	-1.783571	-0.004312
C	-2.563302	-0.720992	-0.510551	H	2.220171	-0.080304	-2.327948				
C	-2.548501	1.31336	0.569371	C	-1.001161	0.510674	-4.234201				

Table A1.3. Optimized geometry of $[Fe(py)_6]^{2+}$.

Lowest Frequency [cm^{-1}]	Minimum Energy [a.u]
26.64	-2753.703819

Table A1.4. Lowest frequency and minimum energy of $[Fe(py)_6]^{2+}$.

$[Fe(C_6H_6N_2)_3]^{2+}$

Atom	Coordinates [Å]			Atom	Coordinates [Å]		
	x	y	z		x	y	z
Fe	-0.15698	0.020654	-0.08917	H	0.770809	5.081996	0.452878
C	-0.106995	-0.533195	2.87884	H	-1.58008	5.595204	1.154613
C	1.931482	-0.205062	1.827837	N	-0.488458	1.968726	0.273162
C	0.52532	-0.737235	4.103898	C	-2.618268	1.076833	0.692383
H	-1.184561	-0.580091	2.796511	H	-3.67322	1.146219	0.945368
C	2.627086	-0.395594	3.017119	N	-2.034357	-0.03546	0.40123
C	1.911102	-0.666745	4.179729	H	-2.636294	-0.85781	0.403564
H	-0.074191	-0.948023	4.980699	C	-0.670595	-1.15266	-2.627349
H	3.708885	-0.33387	3.025265	C	-0.839006	1.150949	-2.809981
H	2.424395	-0.82094	5.120995	C	-0.968052	-1.327671	-3.974339
N	0.568016	-0.270531	1.751239	C	-1.138765	1.049403	-4.167513
C	2.5557	0.066061	0.548492	H	-0.784468	2.116174	-2.324546
H	3.63639	0.127478	0.446923	C	-1.207255	-0.204619	-4.761877
N	1.744089	0.216196	-0.442054	H	-1.009518	-2.326332	-4.392778
H	2.182542	0.382256	-1.346911	H	-1.316383	1.951328	-4.739835
C	-1.769545	2.250386	0.658766	H	-1.440942	-0.308407	-5.814424
C	0.379849	2.989294	0.213563	N	-0.605478	0.079825	-2.04011
C	-2.193595	3.535844	0.980224	C	-0.392287	-2.234228	-1.702336
C	0.024365	4.300503	0.521965	H	-0.406745	-3.272752	-2.023508
H	1.389003	2.746592	-0.091122	N	-0.125702	-1.874278	-0.494465
C	-1.280256	4.583523	0.909856	H	0.081107	-2.631636	0.155285
H	-3.221301	3.705604	3.705604				

Table A1.5. Optimized geometry of $[Fe(C_6H_6N_2)_3]^{2+}$.

Lowest Frequency [cm^{-1}]	Minimum Energy [a.u]
38.87	-2289.036345

Table A1.6. Lowest frequency and minimum energy of $[Fe(C_6H_6N_2)_3]^{2+}$.

$[N(CH_3)_4]^+$

Atom	Coordinates [Å]			Atom	Coordinates [Å]		
	x	y	z		x	y	z
N	-0.593589	0.422393	0.171257	C	-1.154591	0.870951	-1.153677
C	-1.214354	1.232858	1.279929	H	-0.922136	1.925638	-1.290263
H	-2.291841	1.078848	1.261535	H	-0.697119	0.277709	-1.943509
H	-0.979833	2.283142	1.115777	H	-2.232598	0.719771	-1.143603
H	-0.800759	0.897132	2.22929	C	0.9003	0.62312	0.178065
C	-0.905253	-1.037112	0.380594	H	1.290412	0.295708	1.140146
H	-1.986198	-1.165946	0.374701	H	1.333794	0.032157	-0.626882
H	-0.493011	-1.346454	1.33946	H	1.109336	1.680468	0.025268
H	-0.452147	-1.608566	-0.427605				

Table A1.7. Optimized geometry of $[N(CH_3)_4]^+$.

Lowest Frequency [cm^{-1}]	Minimum Energy [a.u]
175.61	-214.250509

Table A1.8. Lowest frequency and minimum energy of $[N(CH_3)_4]^+$.

SF_6

Atom	Coordinates [Å]		
	x	y	z
S	-0.954158	0.085288	0
F	-0.954158	1.690727	0
F	-0.954158	0.085288	-1.605439
F	0.651281	0.085288	0
F	-0.954158	-1.520151	0
F	-0.954158	0.085288	1.605439
F	-2.559597	0.085288	0

Table A1.9. Optimized geometry of SF_6.

Lowest Frequency [cm^{-1}]	Minimum Energy [a.u]
317.09	-997.368483

Table A1.10. Lowest frequency and minimum energy of SF_6.

APPENDIX 2: RESULTS OF THE NBO CHARGES WITH DFT

*Bold values are the average.

$[Fe(NH_3)_6]^{2+}$

hn			n4	fe
0.391	0.390	0.390	-0.867	0.168
0.390	0.392	0.391	-0.867	
0.392	0.391	0.392	-0.867	
0.392	0.390	0.390	-0.867	
0.391	0.392	0.391	-0.867	
0.390	0.391	0.392	-0.867	
	0.391		**-0.867**	**0.168**

Table A2.1. NBO charges of $[Fe(NH_3)_6]^{2+}$.

$[Fe(py)_6]^{2+}$

ha					ca					nb	fe
0.241	0.207	0.240	0.240	0.242	0.045	0.045	-0.216	-0.216	-0.123	-0.379	0.310
0.241	0.241	0.240	0.241	0.218	-0.219	-0.219	-0.119	-0.119	0.036	-0.379	
0.241	0.241	0.241	0.218	0.218	-0.123	-0.219	-0.216	0.036	0.036	-0.371	
0.207	0.241	0.208	0.218	0.243	-0.219	-0.123	0.030	0.036	-0.222	-0.372	
0.207	0.208	0.208	0.243	0.243	0.045	0.030	0.030	-0.222	-0.222	-0.388	
0.207	0.208	0.240	0.243	0.242	0.045	0.030	-0.216	-0.222	-0.123	-0.388	
		0.229					**-0.097**			**-0.380**	**0.310**

Table A2.2. NBO charges of $[Fe(py)_6]^{2+}$.

$[Fe(C_6H_6N_2)_3]^{2+}$

ha			hc	hn	ca			ce	nb	ne	fe
0.212	0.212	0.213	0.223	0.397	0.092	0.092	0.093	0.13	-0.379	-0.434	-0.035
0.249	0.249	0.247	0.224	0.397	0.061	0.064	0.063	0.132	-0.379	-0.436	
0.250	0.246	0.250	0.223	0.398	-0.159	-0.184	-0.156	0.134	-0.371	-0.421	
0.246	0.250	0.249			-0.187	-0.156	-0.185		-0.372		
					-0.129	-0.128	-0.127		-0.388		
	0.239		**0.223**	**0.397**		**-0.063**		**0.132**	**-0.286**	**-0.430**	**-0.035**

Table A2.3. NBO charges of $[Fe(C_6H_6N_2)_3]^{2+}$.

μ²-4,4'-bis([(pyridin-2-yl)methylidene]amino)biphenyl-2,2'-disulfonate ligand

ha		hc	ca		ce	cp	nb	ne	o	s6
0.163	0.186	0.182	0.049	-0.131	0.039	-0.025	-0.367	-0.275	-0.951	2.288
0.165	0.203	0.139	-0.241	-0.256	0.114	-0.043	-0.317	-0.324	-0.975	2.333
0.166	0.167		-0.168	-0.203					-1.021	
0.182	0.192		-0.181	0.102					-0.988	
0.171	0.174		-0.163	-0.247					-0.948	
0.19	0.178		-0.159	0.131					-1.004	
0.201	0.154		0.036	-0.24						
			-0.222	-0.14						
			-0.132	0.03						
			-0.259	-0.264						
0.178		**0.161**	**-0.133**		**0.077**	**0.034**	**-0.342**	**-0.300**	**-0.981**	**2.311**

Table A2.4. NBO charges of μ²-4,4'-bis([(pyridin-2-yl)methylidene]amino)biphenyl-2,2'-disulfonate ligand.

$[N(CH_3)_4]^+$

h1	c3	n4
0.226	-0.386	-0.171
0.226	-0.386	
0.226	-0.386	
0.226	-0.386	
0.226	**-0.386**	**-0.171**

Table A2.5. NBO charges of $[N(CH_3)_4]^+$.

SF_6

s	f1	f2	f3
2.525	-0.421	-0.421	-0.421
	-0.421	-0.421	-0.421
2.525	**-0.421**	**-0.421**	**-0.421**

Table A2.6. NBO charges of SF_6.

APPENDIX 3: RESULTS OF THE LOCAL SCAN WITH DFT AND AILFT: 10Dq AND e_σ

$[Fe(NH_3)_6]^{2+}$

r(Fe-N) [Å]	Energy (DFT) [a.u]	ΔE (DFT) [kcal mol^{-1}]	Energy (AILFT) [a.u]	ΔE (AILFT) [kcal mol^{-1}]	10Dq (DFT) [cm^{-1}]	e_σ (DFT) [cm^{-1}]	10Dq (AILFT) [cm^{-1}]	e_σ (AILFT) [cm^{-1}]
1.83	-1602.760684	9.38	-1600.977867	29.02	44445	14815	29033	9677.7
1.88	-1602.798035	5.47	-1601.053317	21.13	42123	14041	24758	8252.8
1.93	-1602.823434	2.82	-1601.112312	14.96	40001	13334	20907	6968.8
1.98	-1602.839376	1.15	-1601.157895	10.19	37891	12630	17883	5960.8
2.03	-1602.847821	0.27	-1601.192472	6.58	35969	11990	15240	5079.8
2.08	-1602.850356	0.00	-1601.217913	3.92	34248	11416	13128	4376.1
2.13	-1602.848238	0.22	-1601.235691	2.06	32721	10907	11313	3770.9
2.18	-1602.842472	0.82	-1601.247081	0.87	31371	10457	9747.1	3249.0
2.23	-1602.833890	1.72	-1601.253283	0.22	30192	10064	8407.3	2802.4
2.28	-1602.823153	2.84	-1601.255357	0.00	29161	9720.0	7399.7	2466.6
2.33	-1602.810787	4.14	-1601.254170	0.12	28250	9720.3	6334.3	2111.4
2.38	-1602.797241	5.55	-1601.250364	0.52	27460	9416.7	5539.8	1846.6
2.43	-1602.782879	7.06	-1601.244439	1.14	26767	9153.4	4853.9	1618.0

Table A3.1. Local scan of $[Fe(NH_3)_6]^{2+}$.

$[Fe(py)_6]^{2+}$

r(Fe-N) [Å]	10Dq (AILFT) [cm^{-1}]	e_σ (AILFT) [cm^{-1}]	r(Fe-N) [Å]	10Dq (AILFT) [cm^{-1}]	e_σ (AILFT) [cm^{-1}]
1.84	28292	9430.4	2.19	9120.3	3040.1
1.89	23896	7965.3	2.24	7856.9	2619.0
1.94	20073	6690.8	2.29	6791.6	2263.9
1.99	16986	5661.9	2.34	5902.1	1967.4
2.04	14470	4823.3	2.39	5150	1716.7
2.09	12416	4138.7	2.44	4505.9	1502.0
2.14	10648	3549.2			

Table A3.2. Local scan of $[Fe(py)_6]^{2+}$.

APPENDIX 4: RESULTS OF THE MORSE POTENTIAL FIT WITH DFT

$[Fe(NH_3)_6]^{2+}$

r(Fe-N) [Å]	ΔE [kcal mol^{-1}]	r(Fe-N) [Å]	ΔE [kcal mol^{-1}]	r(Fe-N) [Å]	ΔE [kcal mol^{-1}]	r(Fe-N) [Å]	ΔE [kcal mol^{-1}]	r(Fe-N) [Å]	ΔE [kcal mol^{-1}]	r(Fe-N) [Å]	ΔE [kcal mol^{-1}]
1.8	-19.38	2.35	-26.39	2.9	-15.54	3.45	-8.67	4	-4.59	4.55	-1.78
1.85	-23.41	2.4	-25.36	2.95	-14.75	3.5	-8.21	4.05	-4.30	4.6	-1.57
1.9	-26.24	2.45	-24.31	3	-13.99	3.55	-7.78	4.1	-4.01	4.65	-1.36
1.95	-28.11	2.5	-23.24	3.05	-13.27	3.6	-7.37	4.15	-3.73	4.7	-1.15
2	-29.22	2.55	-22.18	3.1	-12.58	3.65	-6.97	4.2	-3.47	4.75	-0.95
2.05	-29.74	2.6	-21.13	3.15	-11.94	3.7	-6.59	4.25	-3.21	4.8	-0.75
2.1	-29.81	2.65	-20.11	3.2	-11.32	3.75	-6.22	4.3	-2.96	4.85	-0.56
2.15	-29.52	2.7	-19.12	3.25	-10.73	3.8	-5.87	4.35	-2.70	4.9	-0.37
2.2	-28.98	2.75	-18.17	3.3	-10.18	3.85	-5.53	4.4	-2.47	4.95	-0.18
2.25	-28.24	2.8	-17.25	3.35	-9.65	3.9	-5.21	4.45	-2.23	5	0.00
2.3	-27.37	2.85	-16.38	3.4	-9.15	3.95	-4.89	4.5	-2.01		

Table A4.1. Morse potential fit for $[Fe(NH_3)_6]^{2+}$.

$[Fe(py)_6]^{2+}$

r(Fe-N) [Å]	ΔE [kcal mol^{-1}]	r(Fe-N) [Å]	ΔE [kcal mol^{-1}]	r(Fe-N) [Å]	ΔE [kcal mol^{-1}]	r(Fe-N) [Å]	ΔE [kcal mol^{-1}]	r(Fe-N) [Å]	ΔE [kcal mol^{-1}]	r(Fe-N) [Å]	ΔE [kcal mol^{-1}]
1.8	12.35	2.35	-23.94	2.9	-17.58	3.45	-9.68	4	-4.37	4.55	-1.37
1.85	3.53	2.4	-23.88	2.95	-16.79	3.5	-9.08	4.05	-4.02	4.6	-1.18
1.9	-3.50	2.45	-23.63	3	-16.00	3.55	-8.50	4.1	-3.68	4.65	-1.00
1.95	-9.06	2.5	-23.23	3.05	-15.23	3.6	-7.95	4.15	-3.36	4.7	-0.83
2	-13.41	2.55	-22.71	3.1	-14.47	3.65	-7.42	4.2	-3.06	4.75	-0.67
2.05	-16.75	2.6	-22.11	3.15	-13.72	3.7	-6.91	4.25	-2.78	4.8	-0.52
2.1	-19.28	2.65	-21.43	3.2	-13.00	3.75	-6.43	4.3	-2.51	4.85	-0.38
2.15	-21.13	2.7	-20.71	3.25	-12.29	3.8	-5.98	4.35	-2.25	4.9	-0.24
2.2	-22.43	2.75	-19.95	3.3	-11.60	3.85	-5.54	4.4	-2.01	4.95	-0.12
2.25	-23.27	2.8	-19.17	3.35	-10.94	3.9	-5.13	4.45	-1.79	5	0.00
2.3	-23.75	2.85	-18.38	3.4	-10.30	3.95	-4.74	4.5	-1.57		

Table A4.2. Morse potential fit for $[Fe(py)_6]^{2+}$.

SF_6

r(S-F) [Å]	ΔE [kcal mol^{-1}]	r(S-F) [Å]	ΔE [kcal mol^{-1}]	r(S-F) [Å]	ΔE [kcal mol^{-1}]	r(S-F) [Å]	ΔE [kcal mol^{-1}]	r(S-F) [Å]	ΔE [kcal mol^{-1}]	r(S-F) [Å]	ΔE [kcal mol^{-1}]
1.3	-31.90	2.15	-67.22	3	-20.09	3.85	-6.04	4.7	-1.98	5.55	-0.58
1.35	-61.71	2.2	-62.96	3.05	-18.68	3.9	-5.65	4.75	-1.86	5.6	-0.53
1.4	-82.07	2.25	-58.89	3.1	-17.37	3.95	-5.28	4.8	-1.74	5.65	-0.48
1.45	-95.34	2.3	-55.03	3.15	-16.15	4	-4.94	4.85	-1.63	5.7	-0.43
1.5	-103.34	2.35	-51.36	3.2	-15.03	4.05	-4.62	4.9	-1.53	5.75	-0.39
1.55	-107.49	2.4	-47.90	3.25	-13.98	4.1	-4.33	4.95	-1.43	5.8	-0.35
1.6	-108.82	2.45	-44.63	3.3	-13.01	4.15	-4.05	5	-1.33	5.85	-0.31
1.65	-108.14	2.5	-41.57	3.35	-12.12	4.2	-3.79	5.05	-1.25	5.9	-0.27
1.7	-106.03	2.55	-38.69	3.4	-11.28	4.25	-3.55	5.1	-1.16	5.95	-0.23
1.75	-102.90	2.6	-36.00	3.45	-10.51	4.3	-3.33	5.15	-1.08	6	-0.19
1.8	-99.09	2.65	-33.48	3.5	-9.80	4.35	-3.12	5.2	-1.01	6.05	-0.16
1.85	-94.83	2.7	-31.14	3.55	-9.13	4.4	-2.92	5.25	-0.94	6.1	-0.12
1.9	-90.29	2.75	-28.95	3.6	-8.52	4.45	-2.74	5.3	-0.87	6.15	-0.09
1.95	-85.60	2.8	-26.91	3.65	-7.95	4.5	-2.57	5.35	-0.80	6.2	-0.06
2	-80.89	2.85	-25.01	3.7	-7.42	4.55	-2.41	5.4	-0.74	6.25	-0.03
2.05	-76.21	2.9	-23.25	3.75	-6.92	4.6	-2.26	5.45	-0.69	6.3	0.00
2.1	-71.64	2.95	-21.61	3.8	-6.47	4.65	-2.12	5.5	-0.63		

Table A4.3. Morse potential fit for SF_6.

APPENDIX 5: d ORBITALS

$[Fe(NH_3)_6]^{2+}$

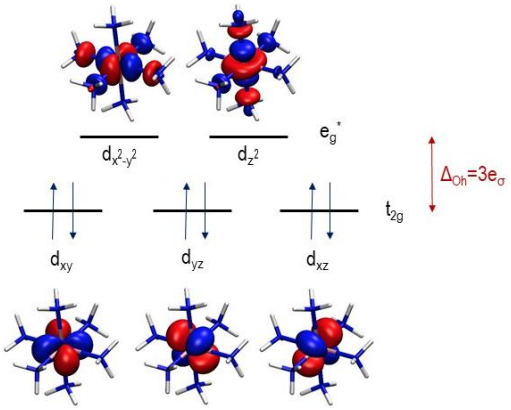

Figure A5.1. d orbitals of $[Fe(NH_3)_6]^{2+}$.

$[Fe(py)_6]^{2+}$

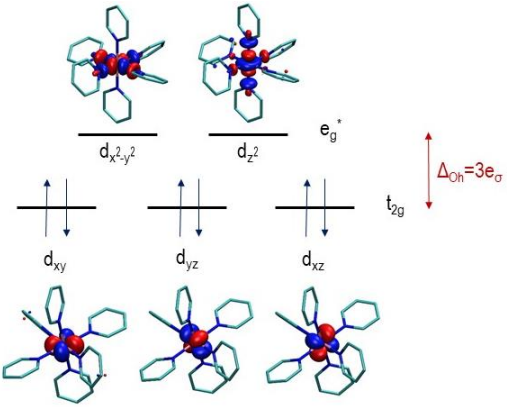

Figure A5.2. d orbitals of $[Fe(py)_6]^{2+}$.

$Fe(C_6H_6N_2)_3]^{2+}$

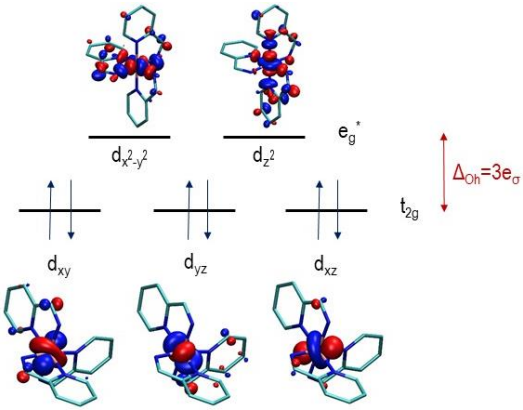

Figure A5.3. d orbitals of $[Fe(C_6H_6N_2)_3]^{2+}$.